6590 *Chem. Mater.* **2010,** *22,* 6590–6597
DOI:10.1021/cm102556h

CHEMISTRY OF MATERIALS
Article

Template Synthesis of Carbonaceous Tubular Nanostructures with Tunable Surface Properties

Shiori Kubo,[†,‡] Irene Tan,[†] Robin J. White,[†] Markus Antonietti,[†] and Maria-Magdalena Titirici*[,†]

[†]*Max Planck Institute of Colloids and Interfaces, MPI Campus Golm, Am Muehlenberg, 14476 Potsdam-Golm, Germany, and* [‡]*National Institute of Advanced Industrial Science and Technology, 16-1, Onogawa, Tsukuba, Japan*

Received September 7, 2010. Revised Manuscript Received November 5, 2010

Uniform, open-ended carbonaceous tubular nanostructures have been synthesized via a hydrothermal route using macroporous anodic alumina membrane (AAO, $d \approx 200$ nm) as template and the biomass derivative 2-furaldehyde as carbon precursor. Surface properties and functionality are controllable via selection of postcarbonization temperature, whereby the material shows increasingly hydrophobic, polarizable character as treatment temperature increases. Surface chemistry and carbon condensation were analyzed by a variety of surface sensitive techniques (i.e., FTIR, Raman, XPS), while tube texture, dimensions and uniformity were examined via gas adsorption studies and electron microscopy. Significantly, the presented synthesis allows access to carbonaceous tubular nanostructures with functional pore walls suitable for the introduction of a wide range of important chemical moieties, including as demonstrated here, the successful grafting of thermoresponsive polymers (e.g., poly-*N*-isopropylacrylamide (PNiPAAm)), providing materials with temperature-dependent hydrophilic−hydrophobic altering behavior and consequent controlled dispersibility in an aqueous phase.

1. Introduction

Carbon nanotubes have attracted a great deal of attention because of their special physicochemical properties, such as confinement and curvature effects, enhanced mechanical and thermal stability, as well as electric conductivity.[1−4] All these important features have led to their application in fields such as sensing,[5,6] photonic crystals,[7] catalyst supports,[8,9] and energy storage.[10,11] Generally, the synthesis of carbon nanotubes relies on relatively harsh conditions such as arcing between two graphite electrodes,[12] or catalytic vapor deposition of hydrocarbon gases in the presence of Fe or Co nanoparticles.[13] These syntheses normally employ high temperatures (e.g., >1000 °C) rendering material chemically inert and hindering facile postchemical functionalization. Commonly, to functionalize conventional carbon nanotubes, a preliminary oxidation step is required using very harsh reagents (e.g., mixtures of HNO_3 and H_2SO_4 acids).[14,15] Thus, while such synthesis and modification strategies can be considered one of the powerful tools, novel approach allowing synthesis of functional carbon nanotubes under mild condition becomes, therefore, of great importance from a process point of view.

A related morphology with partly the same application fields, tubular carbons with larger diameter in the upper nm-range, have been successfully synthesized by using the uniform and straight nanochannels offered by anodic aluminum oxide (AAO) membranes as templates.[16−21] This approach was first introduced by Martin and coworkers who demonstrated the production of metal and polymer microtubles.[22,23] Later on, Steinhart and Wendorff introduced a liquid phase approach to synthesize carbon,

*To whom correspondence should be addressed. E-mail: Magdalena.Titirici@mpikg.mpg.de. Tel.: +49 (0)331-567-9508. Fax: +49 (0)331-567-9502.

(1) Iijima, S. *Nature* **1991**, *354*, 56.
(2) Dekker, C. *Phys. Today* **1999**, *52*, 22.
(3) Forro, L.; Schonenberger, C. *Carbon Nanotubes* **2001**, *80*, 329.
(4) Tomanek, D.; Jorio, A.; Dresselhaus, M. S.; Dresselhaus, G. *Carbon Nanotubes* **2008**, *111*, 1.
(5) Kong, J.; Franklin, N. R.; Zhou, C. W.; Chapline, M. G.; Peng, S.; Cho, K. J.; Dai, H. J. *Science* **2000**, *287*, 622.
(6) Besteman, K.; Lee, J. O.; Wiertz, F. G. M.; Heering, H. A.; Dekker, C. *Nano Lett.* **2003**, *3*, 727.
(7) Lidorikis, E.; Ferrari, A. C. *ACS Nano* **2009**, *3*, 1238.
(8) Zhenhai, W.; Qiang, W.; Jinghong, L. *Adv. Funct. Mater.* **2008**, 959.
(9) Pan, X. L.; Fan, Z. L.; Chen, W.; Ding, Y. J.; Luo, H. Y.; Bao, X. H. *Nat. Mater.* **2007**, *6*, 507.
(10) Tibbetts, G. G.; Meisner, G. P.; Olk, C. H. *Carbon* **2001**, *39*, 2291.
(11) Zandonella, C. *Nature* **2001**, *410*, 734.
(12) Ebbesen, T. W.; Ajayan, P. M. *Nature* **1992**, *358*, 220.
(13) Amelinckx, S.; Zhang, X. B.; Bernaerts, D.; Zhang, X. F.; Ivanov, V.; Nagy, J. B. *Science* **1994**, *265*, 635.
(14) Cui, J.; Wang, W.; P. You, Y.; Z. Liu, C.; H. Wang, P. H. *Polymer* **2004**, *45*, 8717.
(15) Hong, C. Y.; You, Y. Z.; Pan, C. Y. *Chem. Mater.* **2005**, *17*, 2247.
(16) Kyotani, T.; Tsai, L. F.; Tomita, A. *Chem. Mater.* **1995**, *7*, 1427.
(17) Parthasarathy, R. V.; Phani, K. L. N.; Martin, C. L. R. *Adv. Mater.* **1995**, *7*, 896.
(18) Kyotani, T.; Tsai, L. F.; Tomita, A. *Chem. Mater.* **1996**, *8*, 2109.
(19) Rodriguez, A. T.; Chen, M.; Chen, Z.; Brinker, C. J.; Fan, H. Y. *J. Am. Chem. Soc.* **2006**, *128*, 9276.
(20) Wen, Z. H.; Wang, Q.; Li, J. H. *Adv. Funct. Mater.* **2008**, *18*, 959.
(21) Liang, H.-W.; Liu, S.; Yu, S.-H. *Adv. Mater.* **2010**, *22*, 3925.
(22) Martin, C. R. *Adv. Mater.* **1991**, *3*, 457.
(23) Martin, C. R. *Science* **1994**, *266*, 1961.

 Published on Web 11/30/2010 © 2010 American Chemical Society

polymer, or metallic hollow nanotubes.[24,25] This method involves the initial physical wetting of the AAO with the corresponding precursor to form a thin liquid film covering the substrate. After condensation of precursor toward the desired material, the template is removed by acid etching leading to carbon/polymer/metallic nanotubes, where tube diameter can be controlled by the pore size of the template material, while tube thickness corresponds to the amount of wetted monomer. This method has since been extended to the production of 1-D tubular carbon structures from a variety of carbon precursors either by gas[16,18] or liquid[20] infiltration techniques, with subsequent application of the reported materials in a variety of topical fields including catalysis and electrochemistry.[8,18,19,26] Again, the high preparation temperatures involved in the previously reported syntheses of these materials generates tubes possessing limited surface functionality, making the introduction of secondary useful chemical moieties somewhat of a challenge.

The technique of hydrothermal carbonization is a low temperature, solution based, soft chemistry route toward functional carbons[27] and has been previously used in combination with hard templating to produce various porous functional carbon morphologies (e.g., spherical porous beads,[28] ordered mesoporous carbon[29] or carbon monoliths[30]). The utility of this approach to generate functional surfaces has been exemplified by introducing covalent organoamino groups.[29] Here, we extend the combination of hard templating and low temperature hydrothermal carbonization to the replication of macroporous alumina membrane to obtain functional carbonaceous tubular nanostructures suitable for post-chemical modification. It is shown that the surface character of the carbonaceous replicas can be effectively tuned by the post-carbonization temperature allowing the control of surface chemistry from polar (OH, COOH, and C=O functionalities) to increasingly nonpolar states (e.g., extension of the aromatic/pseudographitic nature).

Additionally, we also demonstrate the ease with which chemical moieties can be further introduced by grafting a thermoresponsive polymer (i.e., poly(N-isopropylacrylamide (PNiPAAM)).[31] It is one of the most popular thermoresponsive polymers in biomedical fields due to its lower critical solution temperature (LCST) of 32 °C in water, relatively close to human body temperature. It undergoes sharp reversible hydrophilic−hydrophobic changes in water; by increasing the polymer solution temperature to above 32 °C, the polymer precipitates out of solution. Likewise, PNiPAAm-grafted tubular carbons can be expected to exhibit a very similar hydrophilic−hydrophobic changing behavior, thus being an interesting and promising candidate, for example, as a carrier in controlled catch and release of drug molecules, extending thus the range of potential important applications of carbon materials toward biotechnological and medical fields.

2. Experimental Section

2.1. Materials. Alumina membranes with an average pore diameter of 200 nm (Anodisc 13) were purchased from Whatman International (Maidstone, England). 2-furaldehyde (furfural) was purchased from Sigma-Aldrich (Steinheim, Germany). (3-Aminopropyl)triethoxysilane (APS) was obtained from Fluka. *N*-Isopropylacrylamide (NiPAAm) and 2,2-azobisisobutyronitrile (AIBN) were purchased from Acros and were recrystallized from *n*-hexane and methanol, respectively. The RAFT agent (4-cyanopentanoic acid trithiododecane) was synthesized according to the literature.[32] *N*-Hydroxysuccinimide, *N*,*N*-dicyclohexylcarbodiimide (DCC), and ethyl acetate were also obtained from Fluka.

2.2. Synthesis of Carbonaceous Tubular Nanostructures (Denoted As Tubular Carbons). In a typical synthesis, 0.1 g of alumina membrane (Whatman, Anodisc 13) was soaked in a mixture of 1.2 g of 2-furaldehyde and 4.0 of water, and subsequently placed into a stainless steal autoclave (Parr, Acid Digestion Vessel 4744), which was then sealed and placed in a 180 °C oven for 48 h. The recovered product was washed extensively with water and dried in a vacuum oven overnight at 70 °C. The dried alumina membrane−hydrothermal carbon composite was then further carbonized under an inert atmosphere (i.e N_2) for 4 h at the desired temperatures (i.e., 350, 550, and 750 °C, respectively). To remove the AAO template, a concentrated phosphoric acid washing step was employed, conducted under stirring at 65 °C. The resulting carbon replicas were then sonicated, carefully washed with water and dried in a vacuum oven overnight at 70 °C.

For comparison purposes, impregnation of an AAO membrane was also performed without any previous hydrothermal treatement. Here, alumina membrane was soaked into the mixture of 1.2 g of 2-furaldehyde and 4.0 of ethanol and mechanically shaken at room temperature for 48 h, followed by postcarbonization treatment as indicated above. Template removal was conducted in the same way as described above. In this case, however, no solid precipitate was recovered after washing, proving that the hydrothermal treatment has a crucial role in a successful replication.

2.3. Preparation of Thermoresponsive Tubular Carbons. *2.3.1. Preparation of PNiPAAm in Solution by RAFT.* Four grams (35 mmol) of *N*-isopropylacrylamide (NiPAAm) were dissolved in 6 mL of dry DMF. Forty milligrams (0.1 mmol) of 4-cyanopentanoic acid trithiododecane RAFT agent and 2.6 mg (0.024 mmol) of azobisisobutyronitrile (AIBN) initiator were added to this solution. After three freeze-dry cycles, the reaction mixture was heated at 70 °C for 24 h. PNiPAAm polymer was obtained by precipitation into diethyl ether, followed by drying overnight under vacuum at 50 °C.

(24) Steinhart, M.; Wendorff, J. H.; Greiner, A.; Wehrspohn, R. B.; Nielsch, K.; Schilling, J.; Choi, J.; Gosele, U. *Science* **2002**, *296*, 1997.
(25) Steinhart, M.; Wendorff, J. H.; Wehrspohn, R. B. *Chem. Phys. Chem.* **2003**, *4*, 1171.
(26) Chen, Q. L.; Xue, K. H.; Shen, W.; Tao, F. F.; Yin, S. Y.; Xu, W. *Electrochim. Acta* **2004**, *49*, 4157.
(27) Hu, B.; Wang, K.; Wu, L.; Yu, S.-H.; Antonietti, M.; Titirici, M.-M. *Adv. Mater.* **2010**, *22*, 813.
(28) Titirici, M. M.; Thomas, A.; Antonietti, M. *Adv. Funct. Mater.* **2007**, *17*, 1010.
(29) Titirici, M. M.; Thomas, A.; Antonietti, M. *J. Mater. Chem.* **2007**, *17*, 3412.
(30) Kubo, S.; Demir-Cakan, R.; Zhao, L.; White, R. J.; Titirici, M. M. *ChemSusChem* **2010**, *3*, 188.
(31) De las Heras Alarcón, C.; Pennadam, S.; Alexander, C. *Chem. Soc. Rev.* **2005**, 276–285.
(32) Mitsukami, Y.; Donovan, M. S.; Lowe, A. B.; McCormick, C. L. *Macromolecules* **2001**, *34*, 2248.

2.3.2. Activation of Carboxylated PNiPAAm. Four grams (0.14 mmol) of carboxylated PNiPAAm was activated with 115 mg (1 mmol) of *N*-hydroxy succinimide and 206 mg (1 mmol) of *N*,*N*′-Dicyclohexylcarbodiimide (DCC) in 10 mL of ethyl acetate, and the mixture was stirred at 0 °C for 2 h, followed by stirring overnight at room temperature. The activated polymer solution was filtered, and the polymer was isolated by precipitation in diethyl ether followed by a drying step overnight under vacuum at 50 °C.

2.3.3. Grafting of PNiPAAm onto Tubular Carbons. Seventy milligrams of as-synthesized replica tubular carbons were dispersed in a solution of 0.1 mL of (3-aminopropyl)triethoxysilane (APS) dissolved in 10 mL of dry toluene and refluxed under stirring for 12 h. The amino modified tubular carbons were washed with toluene and methanol, filtered, and dried overnight under vacuum at 50 °C. Afterward, the amino modified tubes were dispersed in 10 mL of dry 1,4-dioxane containing 150 mg of carboxylated PNiPAAm and stirred overnight at room temperature. The resulting PNiPAAm-modified tubular carbons were washed with dioxane and methanol, followed by filtration and drying overnight under vacuum at 50 °C.

2.4. Characterization. Scanning electron microscopy (SEM) was performed using a Gemini Leo-1550 instrument. Transmission electron microscopy (TEM) was performed using an Omega 912 instrument (Carl Zeiss, Oberkochen, Germany). Elemental composition was determined using a Vario El elemental analyzer.Thermogravimetric analysis (TGA) was performed using a NETZSCH TG 209 at a heating rate of 10 K min^{-1} under O_2). N_2 and CO_2 sorption analyses were performed using QUADRASORB SI at 77K and an AUTOSORB-1 at 273K (Quantachrome Instrument), respectively. Prior to measurements samples were degassed at 180 °C for 20 h, except for material obtained directly from hydrothermal carbonization, which was degassed at 100 °C. Surface area was determined using the BET method,[33] while textural properties (e.g., pore volume) were calculated using nonlinear density functional theory (NLDFT) from adsorption data.

FT-IR spectra were acquired using a Varian 600 FTIR spectrometer. FT-Raman spectra were acquired using a WiTec Confocal Raman Microscope α-300. X-ray photoelectron spectroscopy was performed using a Thermo Scientific K-Alpha ESCA instrument equipped with Al K-α monochromatised radiation at a 1486.6 eV X-ray source. Photoelectrons were collected at a take off angle of 90° relative to the sample surface. The measurement was done in a constant analyzed energy mode (CAE) with a 100 eV pass energy for survey spectra and a 20 eV pass energy for high resolution spectra. Charge referencing was carried out by setting the lower binding energy of C1s peaks at 285.0 eV. The atomic percentage was determined from the XPS peak area using the Shirley background subtraction technique and the Scofield sensitivity factors.

The lower critical solution temperature (LCST) was determined by using a turbidimetric photometer (TP1, Tepper Analytik). A 0.3 wt % aqueous solution of PNiPAAm-modified tublar carbons were sonicated for 30 min prior to analysis. Light transmission experiments were performed in the temperature range of 10−50 °C at a rate of 1 °C min^{-1}.

3. Results and Discussion

3.1. Synthesis of Tubular Carbons with Controlled Surface Functionalities. The as-synthesized tubular carbons were denoted as HCT, HCT-350, HCT-550, and HCT-750, where HCT refers to "hydrothermal carbonaceous tubular nanostructures", while the number corresponds to the postcarbonization temperature.

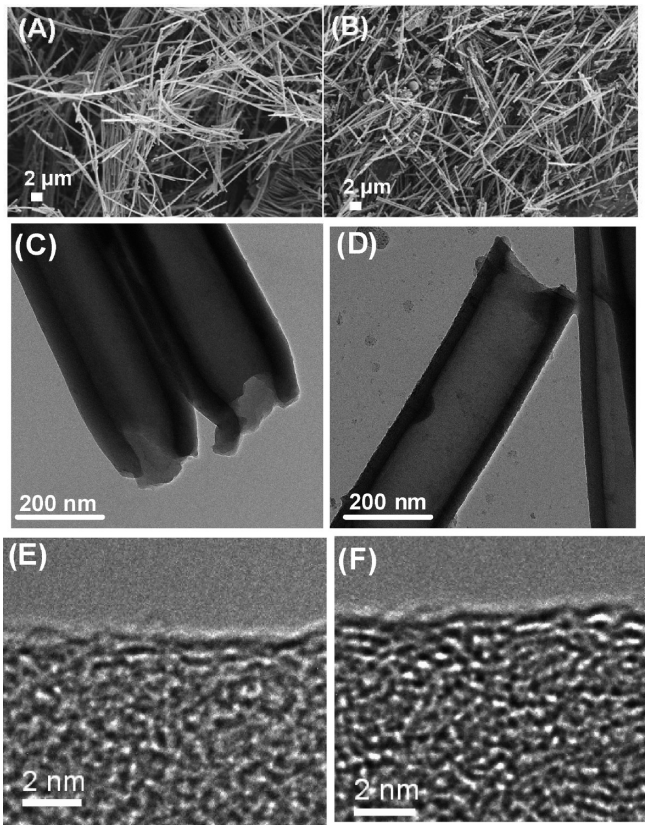

Figure 1. SEM micrographs of synthesized tubular carbons (A) HCT and (B) HCT-750; TEM micrographs of (C) HCT and (D) HCT-750; HR-TEM micrographs of (E) HCT and (F) HCT-750.

SEM micrographs of these samples show in all cases monodisperse tubular structures with a length of several micrometers (Figure 1A and B). TEM micrographs reveal that the tubular carbons possess an open ended structure with smooth surfaces (Figure 1C and D). Tube diameters are approximately equal to size of AAO macropore domains (∼200 nm), constituted of a hollow internal diameter of ∼125(±25) nm and ∼40 nm thick carbonaceous tube walls. All materials, regardless of postcarbonization temperature presented an identical morphology, while pore wall thickness was observed to marginally decrease as treatment temperature passed 550 °C. However, looking carefully at the high-resolution TEM micrographs before (Figure 1E) and after further calcination (Figure 1F), we can observe that the level of local order is improved with temperature. This is also confirmed by the fast Fourier transformation of the HR-TEM images (Figure S2) showing a clearer ring in the case of HTC-750 material. No long-range atomic order translated into an extended aromatic or graphitic layered system could be detected as further confirmed by Raman or XPS spectroscopy, proving that we are dealing with a highly disorderd carbon material.

The successful removal of the alumina template was confirmed using oxidative TGA analysis, indicating a

(33) Brunauer, S.; Emmett, P. H.; Teller, E. *J. Am. Chem. Soc.* **1938**, *60*, 309.

negligible mass residue (e.g., 8.6 wt % for HCT-750; (Figure 2 and Figure S3). dTG curve analysis indicated two main mass loss regions in the case of HCT material, with an initial mass loss event centered around ~300 °C corresponding to the desorption of structural H_2O and CO_2, while the second peak centered at ~440 °C is the result of oxidative corrosion of the carbonaceous framework. The dTG profile of HCT-750 demonstrates much higher oxidation stability as demonstrated by a shift in the peak corresponding to the oxidative event to ~550 °C. Tubular carbons prepared at intermediate carbonization temperatures (i.e., 350 and 550 °C) are increasingly more oxidation stable indicative of the increasing content of aromatic species in the carbon structure (Figure S3). Elemental analysis nicely complements TG analysis, demonstrating the carbon content increase as a function of postcarbonization temperature from 62 wt % for HCT to 81 wt % for HCT-750, while correspondingly the hydrogen and oxygen contents are observed to decrease (Table 1).

One of the most important advantages of the presented synthetic strategy is the possibility to tune the tube surface functionalities via selection of the postcarbonization temperature. To observe changes in the surface chemistry as a function of this preparation parameter, the four synthesized tubular carbon samples were analyzed by FT-IR (Figure 3). Spectra for HCT and HCT-350 present a broad absorption band between 3700 and 3100 cm^{-1}, corresponding to (H-bonding) −OH stretching modes. Additionally bands in the range of 1800 - 1520 cm^{-1} are assigned to C═O stretching modes from C(O)OH/lactone-type groups revealing that the surfaces of these low carbonization temperature replicas are decorated with oxygenated functional groups.[34] Spectra for HCT and HCT-350 also indicate the presence of methyl-type groups (e.g., ν(C−H) stretching mode; 2925 cm^{-1}) and conjugated C═C/olefinic species (C═C−O) (e.g., stretching modes between 1650 and 1450 cm^{-1}). As the carbonization temperature is increased (e.g., @HCT-550), bands associated with C═O features become increasingly weaker, in unison with a decrease in intensity of −OH bands. Heating to 550 °C and above results in an increasingly stronger aromatic character as C−H (out-of-plane) bending modes are observed at 877 cm^{-1}, 816 cm^{-1}, and

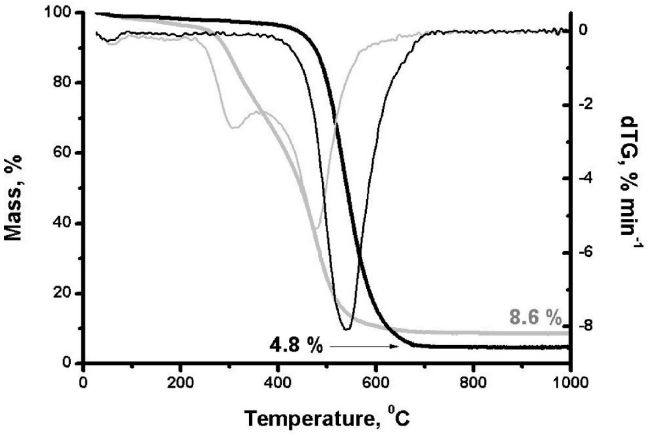

Figure 2. TGA (bold line) and dTG (normal line) curves of HCT (gray) and HCT-750 (black).

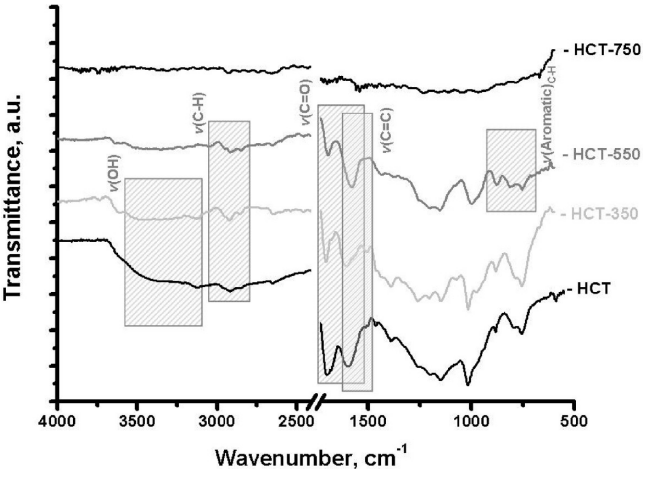

Figure 3. FT-IR spectra of synthesized tubular carbons; HCT, HCT-350, HCT-550, and HCT-750 from bottom to top.

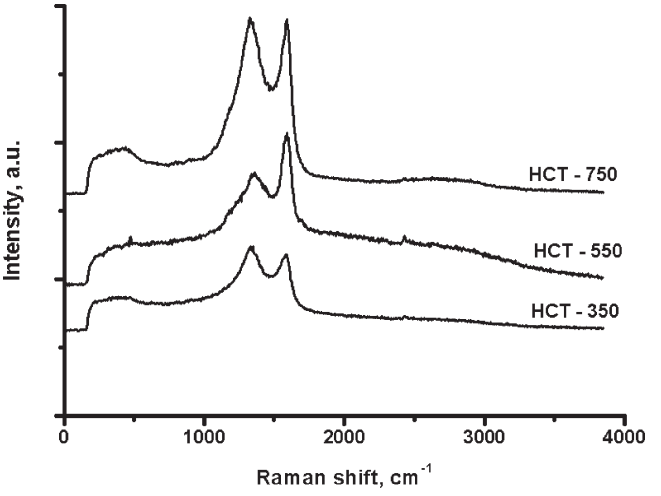

Figure 4. Raman spectra of HCT-350, HCT-550, and HCT-750.

Table 1. Structural and Surface Properties of the Synthesised Tubular Carbons

					N_2		CO_2	
sample	C, %[a]	O, %[a]	N, %[a]	surface functional groups[b]	S, $m^2\ g^{-1}$[c]	V_{total} (V_{micro}), $cm^3\ g^{-1}$[d]	S, $m^2\ g^{-1}$[c]	V_{total} $cm^3\ g^{-1}$[d]
HCT	62	34	0	−OH, C═O, C−H, C═C, C═C−O	33	0.05 (0)		
HCT-350	63	33	0	−OH, C═O, C−H, C═C, C═C−O	22	0.03 (0)		
HCT-550	73	26	0	C═C, C−H, C−H(out-of-plane)	116	0.14 (0.06)	550	0.16
HCT-750	82	16	0.2		699	0.53 (0.12)	674	0.21
HCT-PNiPAAm	61	33	1.5	−OH, C═O, C−H, C═C, C═C−O, −NH				

[a] C, O, N content from elemental analysis. [b] Surface functional groups observed by FT-IR. [c] BET surface area and. [d] Total pore volume with micropore volume in parentheses calculated by NLDFT method.

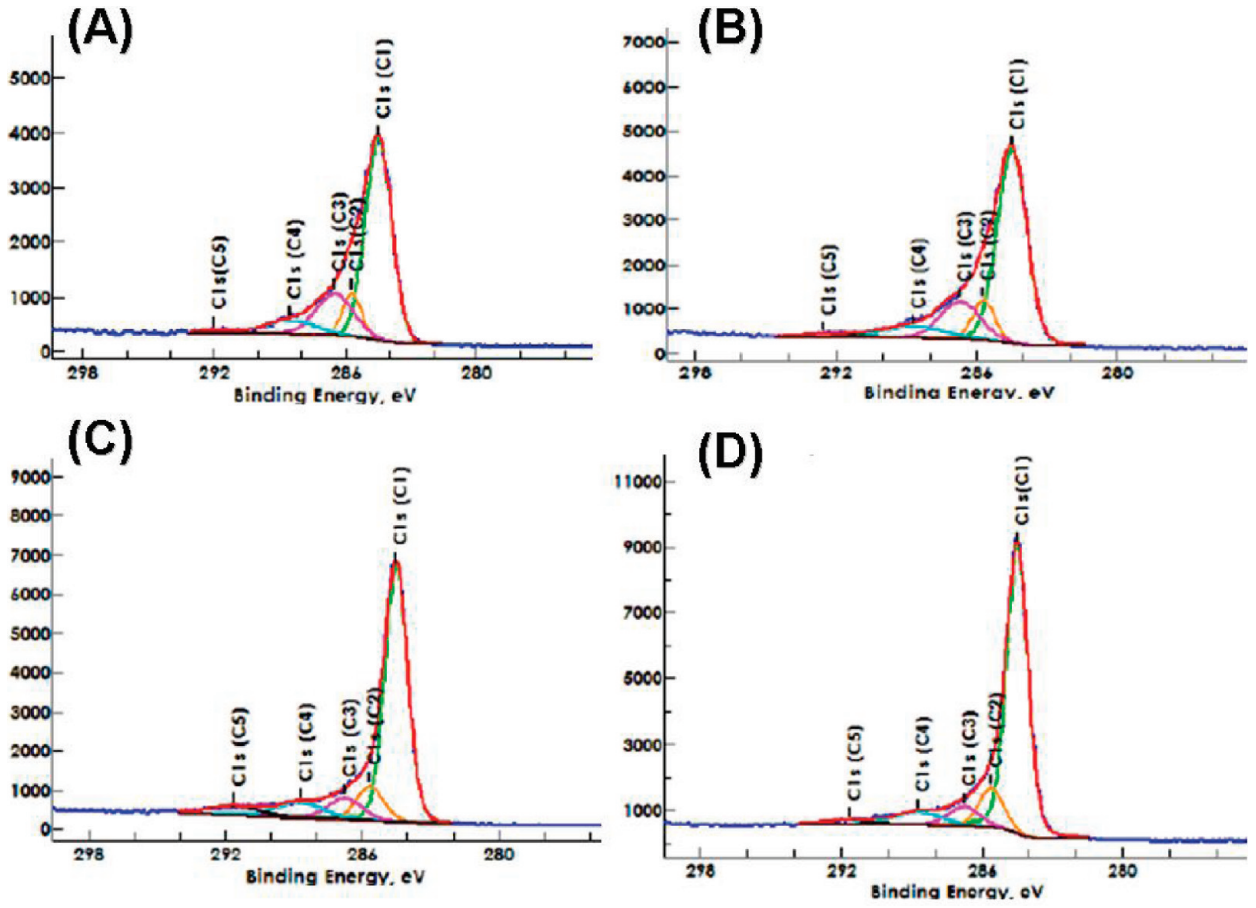

Figure 5. High-resolution XPS scans of C 1(s) photoelectron envelope for (A) HCT, (B) HCT-350, (C) HCT-550, and (D) HCT-750.

752 cm^{-1}.[35] For material prepared at 750 °C, acquisition of suitable spectra was not possible because of the increasingly light absorbing character of the carbon material.

Additionally, Raman spectroscopy confirmed the increase in the aromatic character toward a disordered, graphitic-like structure with the increase in the temperature (Figure 4). All samples examined, even in the case of the HCT-350 material, present typical D (1336 cm^{-1}) and G (1579 cm^{-1}) bands, indicating the presence of disordered carbon and graphitic-like domains.[36] Once the temperature is increased to 550 and 750 °C, respectively, the G band becomes more and more pronounced, indicating structure condensation and aromatization as also confirmed by HR-TEM (Figure 1F).

High-resolution XPS scans of the C 1(s) photoelectron envelope were deconvoluted to examine the varying surface functionality of the presented tubular carbons as a function of postcarbonization temperature (Figure 5). Deconvolution revealed peaks common to all the presented materials, namely a peak corresponding to $-CH_x$/C−C (284.5 eV, **C1**) with an associated $\pi \rightarrow \pi^*$ shakeup satellite (292 eV, **C5**), two peaks related to oxygenated carbon species; C−O (286.7 eV, **C3**) and C═O (288.7 eV, **C4**), and finally a spectral component (285.7 eV, **C2**) included to compensate for the asymmetry of the C 1(s) peak. For HCT material, the C1 peak represents the largest envelope contribution (peak area 62.1%) while C3 (19.0%) and C4 (8.3%) peaks can also be observed confirming the existence of oxygenated surface groups (Figure 5A). Similar C 1(s) spectral features are also observed for HCT-350, indicating still the presence of oxygenated functionalities such as C═O or C−O, although the relative peak areas are slightly reduced (Figure 5B). An increase in postcarbonization temperature results in the C1 peak increasing in intensity in comparison to the other four peaks (Figure 5C), dominating the spectra for HCT-750 material (Figure 5D), which indicates the development of an increasingly condensed carbon structure and the development of an extended aromatic sp^2 pseudographitic motif. Corresponding O 1(s) spectra presented deconvoluted spectral peaks attributed to C═O (O1) and C−O (O2) groups (Figure 6).

Again, by increasing postcarbonization temperature, significant changes in the percentage area ratio for the O1 and O2 peaks was observed, showing increasing spectral dominance for O2 species as the overall material "O" content decreases (Table 2). Elemental composition determined from XPS survery scane are in relatively good agreement with elemental analysis data, the results indicating that with increasing the temperature an increase in the surface carbon content occurs (from 68.9 wt % for

(34) Lua, A. C.; Yang, T. *J. Colloid Interface Sci.* **2004**, *274*, 594.
(35) GomezSerrano, V.; PastorVillegas, J.; PerezFlorindo, A.; Duran-Valle, C. *J. Anal. Appl. Pyrolysis* **1996**, *36*, 71.
(36) Lespade, P.; Aljishi, R.; Dresselhaus, M. S. *Carbon* **1982**, *20*, 427.

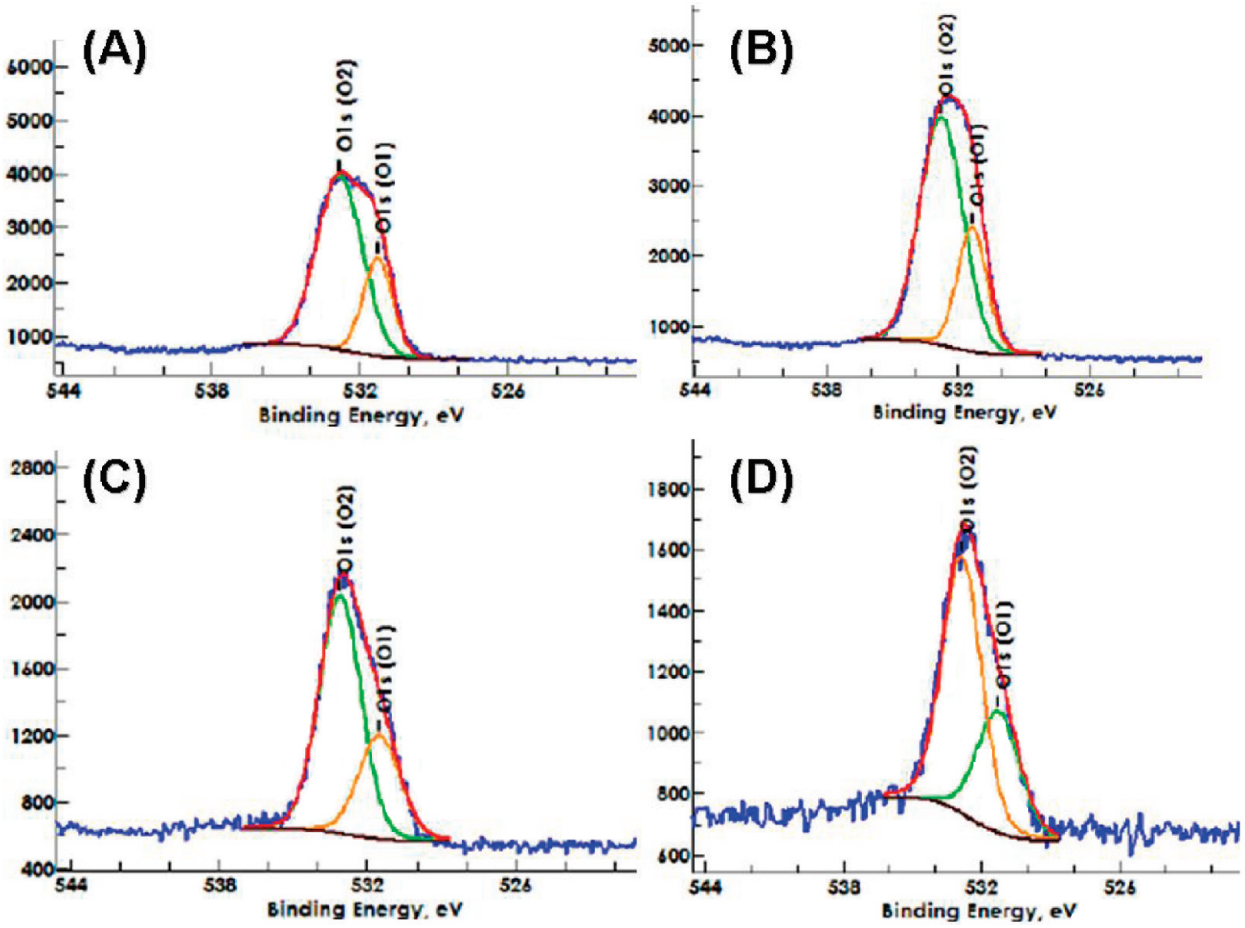

Figure 6. High-resolution XPS scans of O 1(s) photoelectron envelope for (A) HTC, (B) HCT-350, (C) HCT-550, and (D) HCT-750.

Table 2. Peak Area Contributions after Deconvolution of C 1(s) and O 1(s) Photoelectron Envelopes As a Function of Postcarbonization Temperature Treatment

	C 1(s) (% area)					O 1(s) (% area)	
sample	sp^2 [a]	asymmetry [b]	C−O [c]	C=O [d]	$\pi \rightarrow \pi^*$ [e]	C−O [f]	C=O [g]
HCT	62.1	9.3	19.0	8.3	1.3	73.0	27.0
HCT-350	62.8	9.8	16.6	8.4	8.5	72.5	27.5
HCT-550	68.3	10.7	8.3	8.0	4.7	69.5	30.5
HCT-750	73.0	11.3	7.0	6.7	2.4	66.7	32.3

[a] Area percentage of the carbon sp^2 peak in XPS scans of C1(s). [b] Area percentage of the asymmetry compensation peak in XPS scans of C1(s). [c] Area percentage of the C−O peak in XPS scans of C1(s). [d] Area percentage of the C=O peak in XPS scans of C1(s). [e] Area percentage of the $\pi \rightarrow \pi^*$ shakeup satellite peak in XPS scans of C1(s). [f] Area percentage of the C−O peak in XPS scans of O1(s). [g] Area percentage of the C=O peak in XPS scans of O1(s).

HCT to 92.2 wt % for HCT-750) and the amount of oxygen decreases significantly (from 26.5 wt % for HCT to 6.9 wt % for HCT-750) (Table 2). Thus, the surface chemistry (and by implication surface polarity) of these carbonaceous tubular nanostructures can indeed be finely tuned by selection of an appropriate postcarbonization temperature.

The porosity of the tubular carbons was determined using N_2 and CO_2 sorption analysis (Figure 7; Table 1). The HCT and HCT-350 samples showed only negligible pore volume, typical of this open macroporous tubular morphology and of a dense low temperature hydrothermal carbonaceous wall structure. Developed microporosity was found in the materials prepared at elevated temperature (i.e., 550 and 750 °C). The N_2 isotherm of HCT-550 indicates an increase in specific surface area (i.e., 116 $m^2 g^{-1}$) and a total pore volume of 0.14 $cm^3 g^{-1}$ of which 0.06 $cm^3 g^{-1}$ is microporosity accessible to the N_2 molecule. HCT-750 presents a specific surface area of 699 $m^2 g^{-1}$ with a total pore volume of 0.53 $cm^3 g^{-1}$ of which 0.12 $cm^3 g^{-1}$ can be contributed to microporous domains. The degree of microporosity is consistent with that found for normal, nonstructured hydrothermal carbons postcarbonized at 550 and at 750 °C. CO_2 sorption analysis provides complementary characterization of the micropore domains in the presented materials; HCT-550 presents a surface area of 550 $m^2 g^{-1}$ and a total pore volume of 0.16 $cm^3 g^{-1}$, while HCT-750 presents a specific surface area of 674 $m^2 g^{-1}$ and a total pore volume of 0.21 $cm^3 g^{-1}$. Thus HCT-550 shows less microporosity and surface area in N_2 sorption than in CO_2 sorption, while HCT-750 shows relatively comparable values for both analyses. This means that a majority of micropores already exists but is still very small in HCT-550, which then only ripens while further heating to 750 °C.

3.2. Surface Modification of Tubular Carbons with Thermoresponsive Polymer. Among stimuli responsive polymers, poly-*N*-isopropylacrylamide (PNiPAAm) is known to have the sharpest hydrophobic/hydrophilic

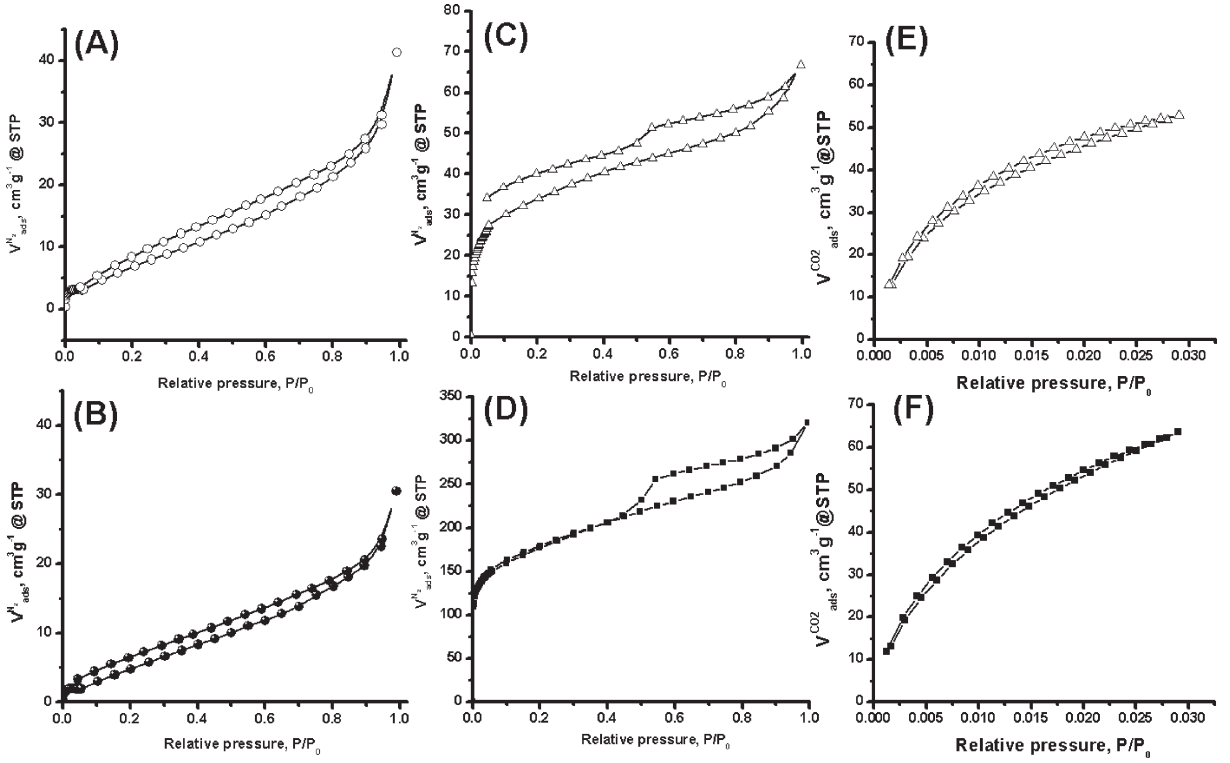

Figure 7. N_2 sorption isotherms for (A) HCT, (B) HCT-350, (C) HCT-550, and (D) HCT-750 and CO_2 sorption isotherms for (E) HCT-550 and (F) HCT-750.

transition at a low critical solution temperature (LCST) of 31−32 °C in aqueous solution.[37,38] This polymer also has been already successfully attached to silica[39] and carbon[40,41] nanostructured materials. In contrast to a silica matrix, a carbon matrix confers greater stability, pH resistivity, and mechanical strength. However, reports thus far described in the literature to produce carbon/thermoresponsive polymer hybrids encounter the previously mentioned problems regarding the functionalization of the surface.[40−43] We have shown in the previous section that HCT possesses a high degree of surface functionality (e.g., −OH, C−O, C═O), confering significant advantages. For potential future applications (e.g., in drug delivery or encapsulation), we therefore demonstrate the simplicity of procedure by attaching PNiPAAm onto the surface of these tubular carbons (termed HCT-PNiPAAm).

PNiPAAm was synthesized using a controlled polymerization technique (RAFT) in the presence of a carboxylated trithioester RAFT agent, namely, 4-cyanopentanoic acid dithiododecane. The molecular weight of the polymer used in our reaction was determined to be 30 000 (g/mol) using GPC.

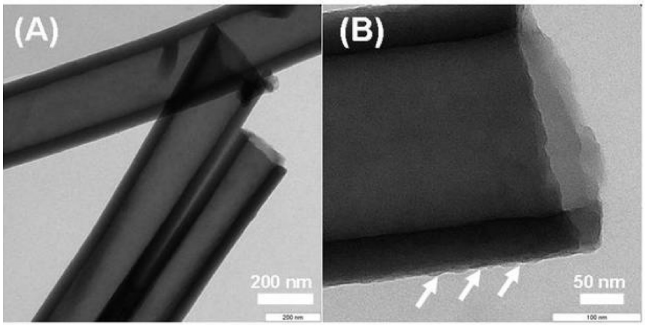

Figure 8. (A and B) TEM micrographs of HCT-PNiPAAm material.

Surface hydroxyl groups of the HCT material were first converted into amino groups via the covalent attachement of the modifier 3-amino propyltriethoxysilane (APS). Then, the previously synthesized carboxyl modified PNiPAAm was coupled to surface amine groups via standard amide bond formation. No significant changes in material morphology as a result of the chemical modification were observed compared to the parent HCT material, and no agglomeration was induced by polymerization (Figure S4). The TEM micrograph indicated maintenance of the tubular nanostructure and dimensions (e.g., diameter ~200 nm; Figure 8A). The higher magnification TEM image indicated the formation of a very thin polymer layer (~2−5 nm) of grafted polymer onto the surface of the tubular carbons which is no longer smooth (see Figure 1), and some roughness can be observed (Figure 8B). Successful grafting of the PNiPAAm was further confirmed by FT-IR analysis, where −NH deformation modes (1565−1475 cm^{-1}) and the increase

(37) Puoci, F.; Iemma, F.; Picci, N. *Curr. Drug Delivery* **2008**, *5*, 85.
(38) Heskins, M.; Guillet, J. E. *J. Macromol. Sci. A* **1968**, *8*, 1441.
(39) Kanazawa, H. *J. Sep. Sci.* **2007**, *30*, 1646.
(40) Xu, G. Y.; Wu, W. T.; Wang, Y. S.; Pang, W. M.; Wang, P. H.; Zhu, G. R.; Lu, F. *Nanotechnology* **2006**, *17*, 2458.
(41) Hong, C. Y.; You, Y. Z.; Pan, C. Y. *Chem. Mater.* **2005**, *17*, 2247.
(42) Strano, M. S.; Dyke, C. A.; Usrey, M. L.; Barone, P. W.; Allen, M. J.; Shan, H. W.; Kittrell, C.; Hauge, R. H.; Tour, J. M.; Smalley, R. E. *Science* **2003**, *301*, 1519.
(43) Bahr, J. L.; Yang, J. P.; Kosynkin, D. V.; Bronikowski, M. J.; Smalley, R. E.; Tour, J. M. *J. Am. Chem. Soc.* **2001**, *123*, 6536.

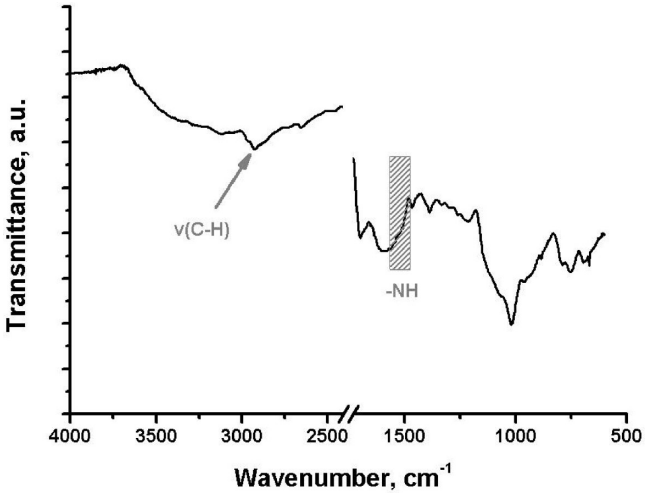

Figure 9. FT-IR spectrum of HCT-PNiPAAm.

in ν(C−H) stretching mode (2925 cm^{-1}) are detected (Figure 9). Elemental analysis indicated an increase in %N compared to the material after APS modification, while a further increase in %N after polymer introduction resulting in a surface grafting density of 1.9 mg m^{-2} (Table 1; See Supporting Information for the calculation).

To test the thermoresponsive behavior of HCT-PNiPAAm, a well-dispersed aqueous solution of the hybrid material was prepared, and light transmission measurements were recorded as a function of temperature cycling in the 15−40 °C range. HCT-PNiPAAm is well dispersed in water below the LCST because of the hydrophilic character of the hybrid. Once the dispersion is heated above 32 °C the hydrogen bonds between the HCT-PNiPAAm and water are disrupted and the tubular carbon material starts to drop out of solution. Indeed, a pure HCT sample in water (0.3 wt %) sediments after two hours at 23 °C, whereas HCT-PNiPAAm sample in water (0.3 wt %) was still well dispersed (Figure S5). Above the LCST (at 40 °C), the HCT sample shows the same behavior as at 23 °C, while the HCT-PNiPAAm hybrid, in contrast, sediments already after 2 h. A full, reversible transsmission hysteresis profile with heating and cooling steps is given in Figure S6. The observed LCST temperature is slightly higher than that of molecular PNiPAAm in aqueous solution because of the covalent attachment of the polymer to the tubular carbon surface and hence an altered molecular architecture.[44] Also the slight broadening of the thermal transition is typical for a brush-like morphology. We are presently investigating the utility of these hybrid materials as potential hollow switchable nanostructures for the encapsulation of bioactive organic molecules.

(44) Roohi, F.; Antonietti, M.; Titirici, M. M. *J. Chromatogr., A* **2008**, *1203*, 160.

4. Conclusion

The successful production of carbonaceous tubular nanostructures via a hydrothermal templating approach has been reported. These materials were synthesized using the hydrothermal carbonization of the sustainable carbon precursor, 2-furaldehyde, in the macropores of an alumina membrane. The flexibility of the reported approach allows access to a wide range of functional materials, with surface functionality/chemistry tunable via selection of postcarbonization treatment temperature. The tubular carbon replicas showed uniform morphology and accessible internal structure via open tube endings. Surface characterization indicated an increasing reduction of the oxygen content of the presented materials, while the aromatic character becomes increasingly prominent as a function of postcarbonization temperature. Tubular nanostructures present accessible macroporosity within the hollow central space, while the carbon tube walls become increasingly microporous as postcarbonization temperature increases. Importantly, as a proof of principle, the model thermoresponsive polymer PNiPAAm was successfully covalently attached to the surface of low temperature hydrothermal carbonaceous tubular nanostructures generating a hybrid material possessing stimuli (thermal) responsive behavior. This feature potentially enables applications in the fields of biotechnology (e.g., enzyme immobilization) and medicine (e.g., as controllable drug microcontainers).

Acknowledgment. S.K. would like to thank DAAD for financial support. Ms. Pitschke and Ms. Runge are thanked for operating SEM and TEM. Dr. Serra at Universidad de Vigo is gratefully acknowledged for performing XPS measurement. Ms. Wilke is thanked for the assistance with CO_2 sorption measurement, and Ms. Shekova is thanked for the performing TGA measurement. The authors would like to thank Dr. Julian Tornow from Fritz Haber Institute of the Max Planck Society for the HR-TEM measurements.

Supporting Information Available: Additional figures and equations. This material is available free of charge via the Internet at http://pubs.acs.org.